Brownian motion of actin filaments in confining microchannels

2005 J. Phys.: Condens. Matter 17 S4091

(http://iopscience.iop.org/0953-8984/17/49/006)

INSTITUTE OF PHYSICS PUBLISHING JOURNAL OF PHYSICS: CONDENSED MATTER

J. Phys.: Condens. Matter **17** (2005) S4091–S4104 doi:10.1088/0953-8984/17/49/006

Brownian motion of actin filaments in confining microchannels

Sarah Köster, Dagmar Steinhauser and Thomas Pfohl[1]

Max Planck Institute for Dynamics and Self-Organization, Bunsenstraße 10, 37073 Göttingen, Germany

E-mail: thomas.pfohl@ds.mpg.de

Received 30 June 2005, in final form 13 September 2005
Published 25 November 2005
Online at stacks.iop.org/JPhysCM/17/S4091

Abstract

Since the cytoskeletal protein actin is one of the principal building blocks of mammalian cells, it has recently been arousing much interest. Here, we address questions concerning the mechanical and dynamic behaviour of individual actin filaments in confining geometries which mimic the dense cytoskeletal network in eukaryotic cells. Microfluidic devices fabricated by soft photolithography in combination with fluorescence microscopy are used to manipulate, observe and characterize these biopolymers. The polymer statistics is strongly dependent on the characteristics of the surroundings such as the degree of confinement and hydrodynamical flow. Besides this, the intrinsic mechanical properties of the filaments are dominated by the persistence length and the contour length. We analyse the tangent–tangent correlation and the radial distribution function in terms of a confining potential and the contour length of the filaments. In addition, we show that hydrodynamic flow can be successfully used to apply controlled local stress on actin filaments. Our results can be surprisingly well described by a straightforward model which approximates the confining energy of the microchannels using a parabolic potential.

(Some figures in this article are in colour only in the electronic version)

1. Introduction

Cell motility, division, shape and mechanical stability of eukaryota are mainly determined by the cytoskeleton, a flexible scaffold made up of a set of fibrous proteins—microtubules, intermediate filaments and actin. They all fulfil very specific tasks in the cell which their structure and mechanical properties are perfectly adapted to. Microtubules, hollow cylinders with a diameter of around 25 nm, are mainly responsible for intercellular transport.

[1] Author to whom any correspondence should be addressed.

Intermediate filaments are ropelike fibres with a diameter of about 10 nm which basically give the cell mechanical strength. Actin filaments have a diameter of about 8 nm and govern, among other things, the cell's motility and shape. Thus, the mechanical and dynamic properties of cytoskeletal proteins and their supramolecular organization are important issues whenever living beings are studied [1]. Actin takes an exceptional position among the three above-mentioned biopolymers. In addition to its considerable importance in life sciences, it also serves as one of the few experimentally accessible model systems for semiflexible chain polymers [2, 3]. A two-stranded helical filament (F-actin) with a diameter of about 8 nm and a helical pitch of 37 nm is assembled from globular actin monomers (G-actin). Since the contour length, L, of the filaments is of the order of several micrometres the fluorescently labelled biopolymers can be observed by optical microscopy. A crucial measure in polymer science is the persistence length, L_{P}. Generally speaking, it is the distance along the contour of the molecule at which two polymer segments have lost any correlation. In a mathematical sense, this is the characteristic decay of the exponential function describing the tangent–tangent correlation of a freely fluctuating filament. Previous measurements on unconfined actin filaments revealed a persistence length of 8–25 μm [2–10]. As this length scale is of the same order of magnitude as the contour length, F-actin is a semiflexible polymer and is situated between stiff biopolymers (e.g. microtubules, $L_{\mathrm{P}} \sim 5.2$ mm [11]) and flexible biopolymers (e.g. DNA, $L_{\mathrm{P}} \sim 50$ nm). Therefore, actin can serve as a model system not only for semiflexible but also for more flexible and stiffer polymers once the contour length is adjusted appropriately. The physical properties of biopolymers are very challenging to investigate *in vivo* and the poor understanding of the mechanical details of the cytoskeleton further complicates a theoretical description of these systems [11, 12]. Therefore, extensive efforts have been made to model the cellular mechanics with purified reconstituted *in vitro* systems. Fortunately, actin can quite readily be polymerized *in vitro* and experiments can be conducted in cell free systems. In recent years, several experimental studies on freely fluctuating actin filaments in dilute solutions have been performed, elucidating some of the mechanical and statistical properties of these biopolymers [2–7]. The dense cytoskeletal network has a mesh size of the order of micrometres and is, on the other hand, exposed to permanent structural changes. It is therefore of substantial interest to look at the individual filament in an environment that resembles its native surroundings [13, 14]. Additionally, the influence of confining geometries, hydrodynamic flow and stress are important for further understanding and design of microfluidic applications in lab-on-a-chip platforms [15–18]. Here, we present investigations and analysis of Brownian motion of individual actin filaments confined in microchannels. The restraining network acting on the individual filament in a cell is mimicked using microfluidic devices. The advantage of this method is that we can fabricate microchannels with a size of the same order of magnitude as the mesh size of the cytoskeleton and additionally a controlled flow can be applied. The experimental method that we use to visualize the actin filaments in the microchannels is standard fluorescence microscopy. We show that the mechanical and dynamic properties of the semiflexible polymers are strongly dependent on both the degree of confinement and the filament length, L. The channel width dependence can be qualitatively described by the standard wormlike chain (WLC) model [19, 20] with an additional energy term considering the confining potential of the channel walls as a parabolic potential. We find the Odijk scaling law for the deflection length, λ, which has been theoretically predicted for circular tubes and a hard wall potential [21], experimentally confirmed. Applying hydrodynamic confinement and stress using a microfluidic focusing device [22] promises to be a powerful method for dynamically manipulating biopolymers. Exerting controlled stress on individual biopolymers, a transition between the fluctuation regime and the complete extension of the filaments can be observed.

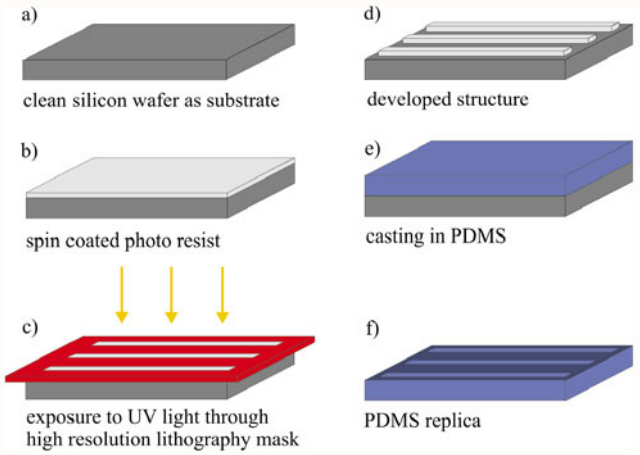

Figure 1. Schematic diagram of the principal steps in soft photolithography.

2. Experimental methods

2.1. Actin polymerization

Lyophilized rhodamine labelled G-actin from rabbit muscle (purchased from Cytoskeleton, Denver, USA) was dissolved in ultrapure water (produced by a Milli-Q Millipore facility) to 10 mg ml^{-1} (in 5 mM tris(hydroxymethyl)aminomethane hydrochloride (tris-HCl) (pH 8.0), 0.2 mM NaATP, 0.2 mM $CaCl_2$, 5% sucrose and 1% dextran). Alexa Fluor 488 G-actin from rabbit muscle, 10 mg ml^{-1} in A-buffer (5 mM tris-HCl (pH 8.0), 0.2 mM NaATP, 0.2 mM $CaCl_2$, 0.5 mM DTT and 0.002% chlorhexidine), was purchased from Molecular Probes, Eugene, USA. Depending on the application, either rhodamine actin or Alexa Fluor 488 actin was used in the experiments. The G-actin solution was diluted in A-buffer to 0.2 mg ml^{-1} and placed on ice for two hours to allow for depolymerization of existing oligomers. Polymerization buffer (100 mM tris-HCl (pH 7.5), 20 mM $MgCl_2$, 500 mM KCl and 10 mM ATP) was added to initiate the polymerization process and the solution was incubated at room temperature for two hours (volume ratio A-buffer:polymerization buffer = 9:1). The solution was diluted to a final monomer concentration of 70 nM in stabilization buffer to prevent the actin filaments from depolymerizing (A-buffer, polymerization buffer (9:1) and 70 nM phalloidin). The solution was thoroughly mixed and kept at 4 °C until it was used for the experiments. To avoid photobleaching and breakage of the filaments during observation, antifade solution (30 mM glucose, 10 mM DTT, 4 μM glucose oxidase, 0.2 mM NaATP, 5 mM tris-HCl (pH 8.0), 2 mM CaCl and 210 units ml^{-1} catalase) was added to the actin solution just before filling the microchannel chamber (volume ratio actin solution:antifade = 5:1).

2.2. Lithography

The microchannels were fabricated using standard soft lithography techniques [23, 24]. In figure 1 the principal steps of this technique are shown. Silicon wafers were cleaned with isopropanol and spin coated with a thin layer (1.4–30 μm) of SU-8 negative photoresist (Micro Resist Technology GmbH, Berlin, Germany). The photoresist was then selectively exposed to UV light through a high resolution chrome mask or lithography transparency and developed. PDMS (poly(dimethylsiloxane)) was poured onto the three-dimensional microstructures and

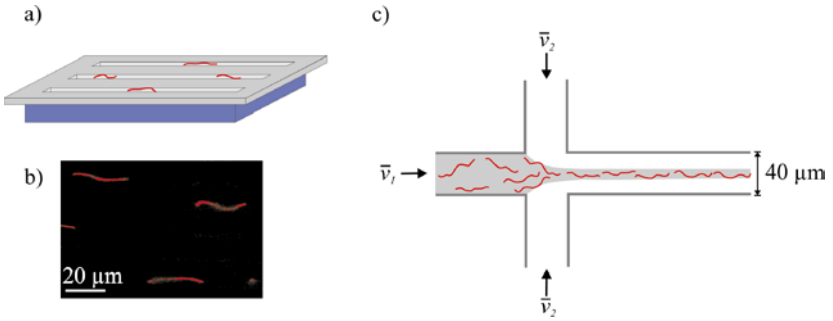

Figure 2. (a) Schematic diagram of a microfluidic device combining many straight parallel channels with different widths, d, which allow for observation of multiple filaments at the same time. (b) Fluorescence micrograph of multiple actin filaments confined in parallel microchannels. (c) Schematic diagram of the crossed channel hydrodynamic focusing and diffusive mixing device.

cured. The PDMS replicas were used for the experiments. A great advantage of using this technique is the rapid turn-around time from conception of the experiment to fabrication. Also, one silicon master can be used many times to fabricate replicas which makes the method very cost-effective and time-effective. To obtain closed channel systems, the PDMS microstructures were plasma oxidized and irreversibly bound to glass coverslips, which provides a tight seal. To avoid adhesion of the actin filaments to the channel walls, the channel surfaces were coated with the protein BSA (bovine serum albumin, 1 mg ml^{-1}) prior to filling the chamber with the dilute F-actin solution which saturates the PDMS and glass surfaces. We found that the filaments were fluctuating inside the channels without sticking for at least 24 h. Experiments without externally applied flow were conducted in parallel channels with varying width, $d = 2$, 4, 6 and 10 μm (figures 2(a) and (b)). Here, only data obtained from chambers with negligible intrinsic flow rates which had no influence on the dynamics of the filaments were analysed. To allow application of a controlled flow and stress to the biopolymers a hydrodynamical focusing device was used [22]. This device will also eventually serve to diffusively intermix actin filaments and actin binding proteins or network forming multivalent ions. The device consisted of two perpendicularly crossed channels [13, 25] which had a depth of 30 μm and a width of 40 μm (figure 2(c)). Computer controlled step motor syringe pumps were connected to the channels via polyethylene tubing. A dilute aqueous actin solution was flowing into the main channel (mean flow velocity $\overline{v}_1$) and was hydrodynamically focused by water flowing into the side channels (mean flow velocity $\overline{v}_2$).

2.3. Microscopy

To investigate the statistical mechanics of individual actin filaments, we observed the contour fluctuations of the biopolymers with an Olympus BX61 fluorescence microscope equipped with a 75 W xenon lamp, a 100× Plan Apochromat oil immersion objective (NA 1.40) and the appropriate filter sets for the fluorescent dyes (rhodamine and Alexa Fluor 488). Movies were recorded using a PCO SensiCamQE CCD camera. For the observation of actin fluctuations without flow the exposure time was 100 ms, 10 frames per second were recorded (see figure 3). Since the visualization of the filaments in the crossed channel device requires very short exposure times, we combined a reduced exposure of 5 ms with 4 × 4 binning in the case of hydrodynamic confinement and stress. The microscopy images were binarized and skeletonized to a one-pixel line using commercial image processing software (Image-Pro

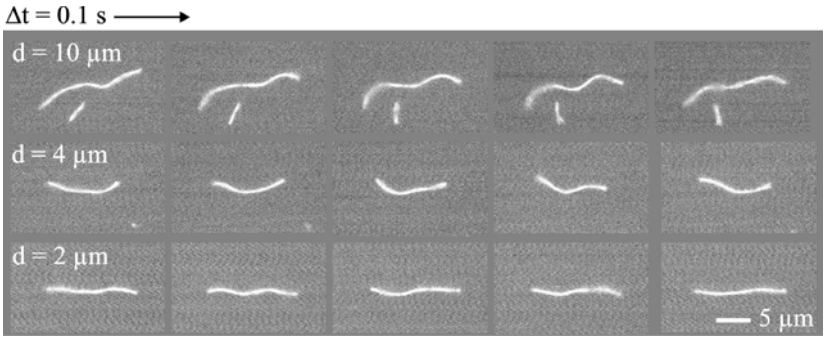

Figure 3. Temporal evolution of fluctuations of actin filaments in channels of different widths.

Plus, AnalySIS, MATLAB). To determine the tangent–tangent correlation, a smoothing spline fit was applied to the one-pixel line. An arc length reparametrization of the fitted line was obtained by dividing it into tangent vectors of equal length. The correlation of these tangent vectors as a function of the arc length, l, is given by their scalar product. We carefully adjusted our experimental system in order to enhance the reliability and reproducibility of the results. The width of the microchannels (2, 4, 6 and 10 μm) covered one order of magnitude, whilst their length (2 cm) guaranteed translational invariance in the direction of the channels. F-actin naturally has a polydisperse length distribution. Since we used a microfluidic chamber which included different channel widths, we were able to investigate the channel width dependence and contour length dependence in a single experiment. An actin concentration of 70 nM was chosen to secure investigations of individual actin filaments avoiding interactions between actin filaments. We observed F-actin in a quasi-2D system. Without external flow this was obtained by using channels which had a depth of merely 1.4 μm. In the case of hydrodynamic confinement and stress the channels were deeper (30 μm). In both cases, we observed the 2D projection of the filaments into the focal plane of the microscope which is possible because the filaments' fluctuations out of this plane are small.

3. Results and discussion

3.1. Theoretical description of semiflexible polymers

Since the persistence length of semiflexible polymers is of the same order of magnitude as their contour length, they cannot be described by Gaussian statistics. Instead, the wormlike chain (WLC) model [19, 20] is used to describe this class of polymers. The Hamiltonian describing the mechanical properties of the system only contains the bending free energy of the chainlike molecule:

$$H = \frac{\kappa}{2}\int_0^L \mathrm{d}l \left[\frac{\partial^2 \mathbf{r}(l)}{\partial l^2}\right]^2, \tag{1}$$

where L is the contour length of the filament, κ is the bending rigidity and $\mathbf{r}(l)$ is the position vector on the contour of the filament. The correlation of the tangent vectors $\mathbf{t}(s) = \frac{\partial \mathbf{r}(s)}{\partial s}$ can be calculated in a straightforward manner and is a first-order exponential decay with the persistence length, L_P, as the characteristic length scale [19] (see the dotted line in figure 4):

$$\langle \cos\theta(l)\rangle \equiv \langle \overline{\mathbf{t}(s)\cdot\mathbf{t}(s+l)}\rangle = \exp\left(-l/2L_\mathrm{P}\right), \tag{2}$$

where θ is the angle between the two tangent vectors considered. The bar in equation (2) denotes the spatial averaging within the same image whereas the brackets denote the thermal

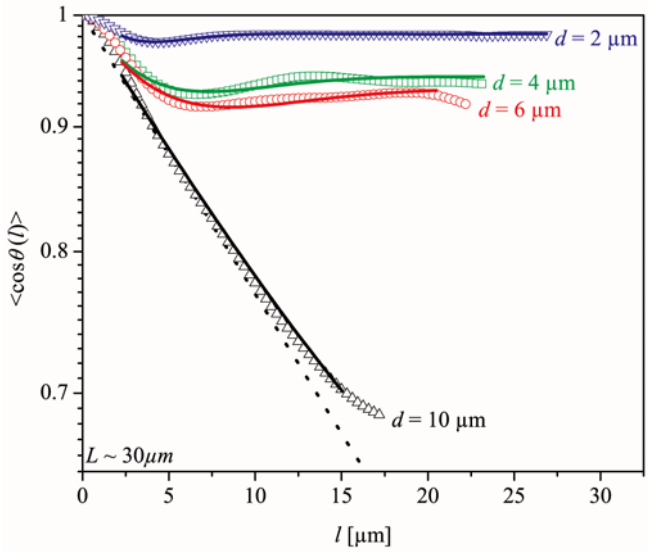

Figure 4. Tangent–tangent correlation functions of actin filaments confined in channels of different widths. Open symbols: experimental data; solid lines: fit using equation (3), where the persistence length is kept constant at $L_P = 19\ \mu$m and the only fitting parameter is the deflection length λ; dotted line: ideal tangent–tangent correlation of a freely fluctuating filament.

(i.e. time) averaging which includes many conformations of a filament. Our experimental set-up physically confines the filaments to two dimensions and we observe the projection of the filaments' fluctuations merely in the focal plane of the microscope. Therefore, the theoretical description has to be adjusted to the two-dimensional case as well. This leads to the factor 2 in the denominator of the exponent. In experiments without confining channels (data not shown), $L_P = \kappa/k_BT = 19\ \mu$m for freely fluctuating actin filaments was measured. The WLC model is merely based on the mechanics of the actin filaments. For our system an additional energy term describing the confining microchannels has to be accounted for and included in a modified WLC model. Ideally, this should be a hard wall potential implying rectangular channels. However, we found that even a very rough estimate using a parabolic wall potential $\frac{K}{2}z(l)^2$, where the z-axis is perpendicular to the direction of the channels and K is a constant value determining the strength of the potential, describes our experimental results surprisingly well [26]. A great advantage of this model is that the tangent–tangent correlation can be analytically obtained:

$$\langle \cos\theta(l) \rangle = 1 - \frac{\lambda}{\sqrt{2}\,2L_P}\left(\cos\left(\frac{\pi}{4}\right) - \cos\left(\frac{\pi}{4} + \frac{l}{\lambda}\right)\exp\left(\frac{-l}{\lambda}\right)\right). \qquad (3)$$

In addition to L_P which describes the mechanical rigidity of the actin filaments, a second parameter is now introduced: the deflection length, $\lambda = (4\kappa/K)^{1/4}$, which is characterized by the competition of bending energy and confining energy. A descriptive idea of the deflection length as the distance between two consecutive contact points of the filament with the channel walls and the appropriate scaling law has been introduced by Odijk [21]. Note that these scaling arguments, as well as more rigorous calculations of the deflection length, were deduced for semiflexible filaments in cylindrical hard wall tubes of diameter d [21, 27, 28], whereas a parabolic potential was used to describe our system. In order to highlight this rather important difference, we name the scaling factor deduced from the hard wall model λ_H in the following.

However, λ shows the same scaling behaviour as λ_H. For large distances l, the tangent–tangent correlation described by equation (3) approaches a constant asymptotic non-zero value:

$$\langle \cos\theta(l) \rangle \approx 1 - \frac{\lambda}{4L_P} = \text{const} \neq 0. \tag{4}$$

The ramification of this unique characteristic is that the tangential orientations of two polymer segments which are far apart from each other seem to be very well correlated (in contrast to the free tangent correlation case where they are not correlated at all). This is however not a direct coupling of the segments as in the case of stiffer polymers with larger persistence lengths. All segments are coupled to the external channel potential and thus merely indirectly coupled to each other. The external confining potential thus serves as a micrometre scale track for the polymer. As a matter of principle there is a noteworthy difference: the tangent–tangent correlation of stiffer polymers which are freely fluctuating without any confining microchannels (e.g. microtubules) still shows an exponential decay, but the persistence length is larger and thus the decay is weaker. Here, in contrast, we observe a characteristic oscillation along the tangent–tangent correlation whose wavelength is set by the external potential. Determining the position of the first local minimum of the modified tangent–tangent correlation (equation (3)), we find that it depends on the deflection length but not on the persistence length:

$$\lambda = \frac{2}{\pi} l_{\min}. \tag{5}$$

This provides a suitable method for deducing the deflection length from the experimental results.

To show the principal difference between Gaussian and semiflexible chain molecules it is instructive to compare the respective radial distribution functions. For Gaussian chains it can for many purposes be well approximated by a normal probability curve. For semiflexible polymers the description is somewhat more complex. Nevertheless, for a given contour length, L, and persistence length, L_P, the approximate radial distribution function, $G_0(R/L)$, for free semiflexible polymers can be calculated analytically [29]:

$$G_0(R/L) = \frac{2L_P}{4L\pi\mathcal{N}} \sum_{k=1}^{\infty} \pi^2 k^2 (-1)^{k+1} \exp\left(-\frac{L_P}{L} \pi^2 k^2 (1 - R/L) \right), \tag{6}$$

where $\mathcal{N}$ is a normalization constant. Analysing the radial distribution function provides a second method for obtaining the persistence length from the experimental data and thus verifies the consistency of the experiment and the data analysis. Combining the two statistical measures, the tangent–tangent correlation and the radial distribution function, helps to complete the characterization of semiflexible polymers.

3.2. Influence of the confining potential on fluctuating actin filaments

In figure 4 semi-logarithmic plots of the tangent–tangent correlations for fluctuating filaments in microchannels of different widths (2, 4, 6 and 10 μm) are shown. A minimum contour length of $L \sim 30$ μm was chosen for this analysis to ensure that the contour length of the filaments is large compared to the channel width. The dotted line marks the ideal tangent–tangent correlation of a freely fluctuating filament ($L_P = 19$ μm) in two dimensions. The open symbols show the experimental results [26] which have been fitted using equation (3) (solid lines). Clearly, filaments confined in 10 μm channels ($L \sim 3d$) are not very strongly influenced by the channel geometry; they show almost the same behaviour as free filaments and may even be fitted using the standard WLC model. However, for the smaller channels ($d \leqslant 6$ μm) a strong influence of the restraining channel walls is observed. We observe an overall increasing

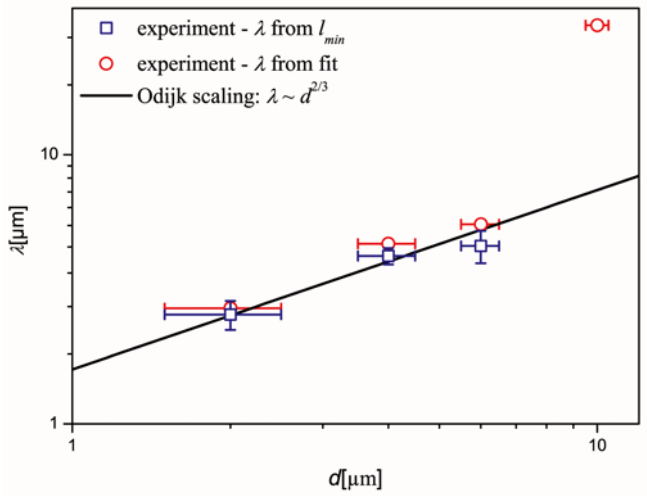

Figure 5. Deflection length λ plotted against the channel width d.

correlation with decreasing channel width. In addition, a local minimum is developed at $l_{\min}$, followed by an oscillation about a saturation level which is finally reached for large l. For large l the correlation reaches a large asymptotic value, instead of dropping to zero as for unconfined filaments. This asymptotic value increases with decreasing channel width, whereas the distance $l_{\min}$ decreases with decreasing channel width. The tangent–tangent correlation shows a small but nevertheless observable deviation from the theoretical curve (equation (3)): it does not decay with a finite but with a zero slope for small l. For this reason only data points for $l \geqslant 2.2$ μm were included when fitting the data using equation (3) with $L_{\mathrm{P}} = 19$ μm. Obviously, the fit for the smallest channels ($d = 2$ μm) is best. In the WLC model, generally infinitely long filaments are assumed. This approximation is best realized for a high ratio of filament length and channel width (>15 in the case of the 2 μm channels). The whole course of the curve can be fitted if an intrinsic non-linear stiffness of the filament chain is assumed and included in the theoretical model, avoiding radii of curvature smaller than a certain minimum value. This feature can be taken into account by introducing a finite cut-off length considering higher terms in the bending energy [30].

We are aware of the fact that the tangent–tangent correlation reacts sensitively to parameters used for data analysis such as the digitization of the contour of the filaments, and the polynomial order and strength of the applied smoothing spline. To verify the consistency of our experimental results and the model used for data analysis, the deflection length was deduced from the data using two different methods. First of all, the local minima of the data curves (figure 4) were determined. Using equation (5), values for λ were obtained. Secondly, the whole data set was included to identify λ as it is the free fit parameter in equation (3). In figure 5 the results from both methods of analysis for λ are plotted. In addition, the Odijk scaling law $\lambda \sim d^{2/3}$ is shown [21] (solid line). Since the data for the 10 μm channels do not display a local minimum, we can only show the value from the fit in this case. The value is not in agreement with the scaling law, which supports the above mentioned assumption that filaments in 10 μm channels are merely weakly confined. The values for λ for channel widths 2, 4 and 6 μm are in good agreement for both methods of analysis and with the predicted scaling law. This shows that we chose stable parameters for our data analysis and that the parabolic potential we used for the model is a simple but effective estimate. The scaling law is confirmed;

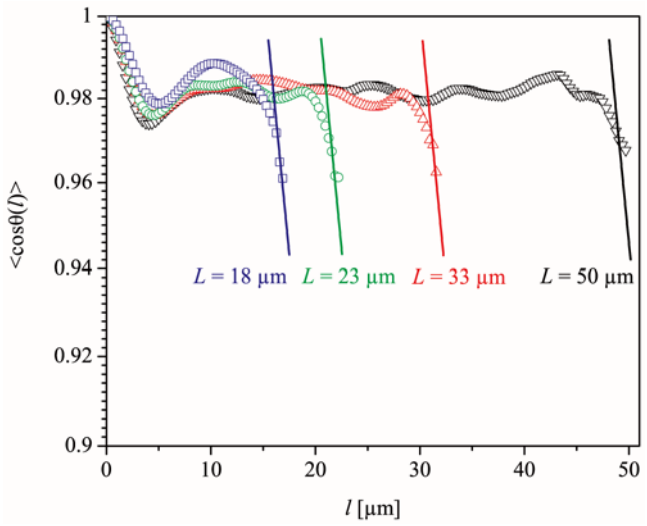

Figure 6. Tangent–tangent correlation functions of actin filaments of different contour lengths confined in a 2 μm channel. Open symbols: experimental data; solid lines: free persistence length $L_P = 19$ μm.

just the coefficient differs from what has been calculated for circular tubes and a hard wall potential [27, 28]. We assume that this discrepancy may be attributed to approximating the confining geometry by a parabolic potential. In turn, the shape and structure of the confining potential which is used plays an important role in setting λ as a characteristic length scale.

3.3. Contour length dependence and radial distribution function

The data shown in figure 4 were averaged over several filaments having approximately the same contour length fluctuating in a channel of the same width in addition to the spatial averaging within the same image and a time dependent averaging including all images of one movie. This was done to improve the statistical reliability of the results and remove fluctuations due to slight differences between individual filaments (e.g. imperfections in the build-up of the polymer). In contrast, in figure 6 each data set represents one individual filament and is only averaged over all conformations of this filament. The contour lengths are different (18, 23, 33 and 50 μm) and the channel width is kept constant at 2 μm. The principal courses are the same for all four data sets. For small values of l we observe a decay which leads to a minimum, followed by oscillations. The length of this oscillation regime depends on the length of the filament. The oscillations are followed by a strong decay. For the analysis displayed in figure 4 all data following the constant plateau have been disregarded. This is necessary because not all filaments have exactly the same contour length and the decay consequently occurs at different positions. It can be seen in this plot that the oscillations are damped when data for more than one filament are averaged. The slope of the tangent–tangent correlation here approaches the typical exponential function of freely fluctuating filaments with persistence length $L_P = 19$ μm as indicated by the solid lines in figure 6. This quasi-free behaviour on a length scale of the order of the channel width is due to the finite length of the filaments. Monte Carlo simulations support this assumption [31]. In the WLC model infinitely long filaments are assumed. This is why this decay cannot be accounted for in the theoretical curves in figure 4, where we disregarded this decay to allow averaging the data and for better comparison with the theoretical description.

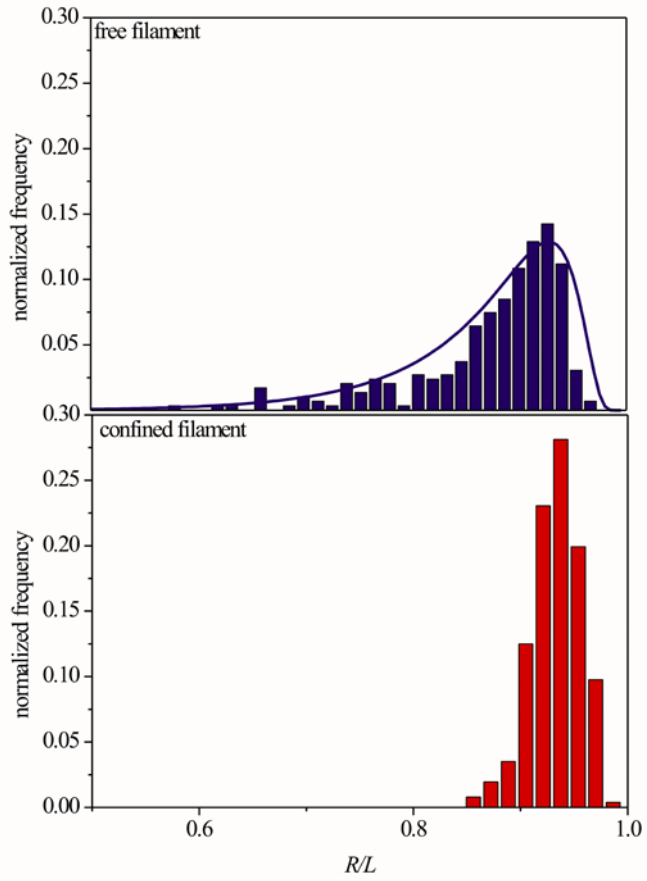

Figure 7. Radial distribution function of a free (top) and a strongly confined (bottom, $d = 1.5\ \mu$m) actin filament; solid line: fit using equation (6).

In addition to the tangent–tangent correlation, the radial distribution function is an important statistical measure in polymer science. Experimentally, it might be easier to obtain only specific points along the filaments' contour rather than the whole contour line. However, small imperfections or defects that yield kinks in the shape of the polymer have a strong influence on the global radial distribution function while they tend to even out for the local tangent–tangent correlation. In figure 7 the normalized radial distribution function for a free (top) and a strongly confined filament ($d = 1.5\ \mu$m, bottom) are shown. Each data set stems from one single actin filament and we recorded 150–300 conformations. The statistics of our results might be moderate in comparison to the data shown in figure 4, but nevertheless the results are in good agreement with the theoretical description which we show by fitting the data for the unconfined semiflexible polymers using equation (6) (solid line in the top image [29]). The persistence length we obtain is $L_P = 18\ \mu$m which is in good agreement with the result deduced from the tangent–tangent correlation of unconfined filaments. When the filament is confined, the distribution function gets narrower and the maximum is shifted to larger values of R/L where R is the distance between the observed points—in our case the end points of the filament—and L is the contour length between them.

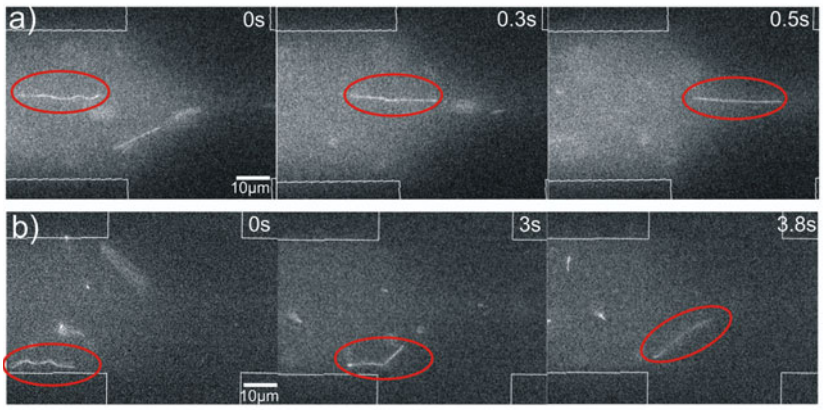

Figure 8. Snapshots of individual actin filaments in extensional flow.

3.4. Hydrodynamic confinement and stress

Hydrodynamic confinement with an extensional flow profile was generated by a hydrodynamic focusing device consisting of two perpendicularly crossed channels (figure 2(c), [22]). An incoming flow ($\overline{v}_1 \sim 20\ \mu\text{m s}^{-1}$) of a dilute aqueous actin solution was hydrodynamically focused by water streams from the two side channels ($\overline{v}_2 \sim 5\overline{v}_1$). Snapshots of the course of individual actin filaments along the hydrodynamic focusing velocity profile are shown in figure 8. A fluctuating actin filament flowing in the centre of the main channel senses a local velocity increase approaching the focusing area (figure 8(a)). At a specific hydrodynamic stress the Brownian motion of the filament is restrained and straightening of the filament can be observed. Owing to the velocity profile in the main channel, actin filaments close to the microchannel walls have a reduced average velocity (figure 8(b)). Nevertheless, on reaching the area of increasing hydrodynamic stress, the fluctuations of the filaments are suppressed as well. The straightened filament is following the streamlines of the hydrodynamic focus.

The velocity profile in this hydrodynamic focusing device was modelled using the finite element method (figure 9). The incompressible Navier–Stokes equation was solved in two dimensions to obtain a stationary solution (low Reynolds number, $Re < 0.1$) using about 20 000 elements (commercial software Femlab). As expected, a parabolic velocity profile perpendicular to the flow direction can be obtained in the channels. At the confluence of the three inlet channels, the flow patterns are interfering, and focusing of the main liquid stream as well as concurrent acceleration of the flow velocities can be observed.

For a first analysis, the extension of the filaments depending on the strain rate, $\dot{\varepsilon}_x$, can be calculated using the simulated velocity field. In order to account for a local change of the flow velocities along the contour of the filament with the two end points P_1 and P_3, the contour length, L, is divided into two segments of equal length, L_S ($L = 2L_S$), by the contour point P_2. The normalized extension, R_{ij}/L_S, is described as the distance R_{ij} of two consecutive points P_i along the contour normalized by the segment length, L_S (figure 10(b)). Since the course of a filament which is flowing in the centre of the main channel (figure 8(a)) is analysed, contributions from a velocity gradient perpendicular to the flow direction are neglected ($\frac{\partial v_y}{\partial y} \sim 0$). Only the components along the flow direction are taken into account to calculate the strain rate, $\dot{\varepsilon}_x = \frac{\partial v_x}{\partial x}$. The dependence of the normalized extension, R_{ij}/L_S, on the strain rate, $\dot{\varepsilon}_x$, is shown in figure 10(a). At $\dot{\varepsilon}_x \sim 0$ Brownian motion is dominating, which

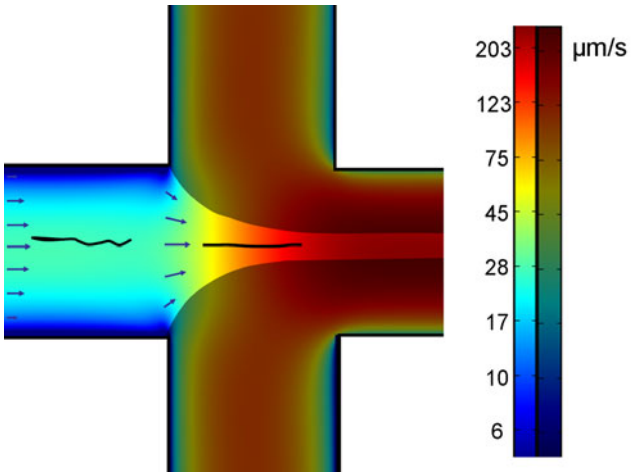

Figure 9. Two-dimensional finite element method simulation of the velocity field in a hydrodynamic focusing device.

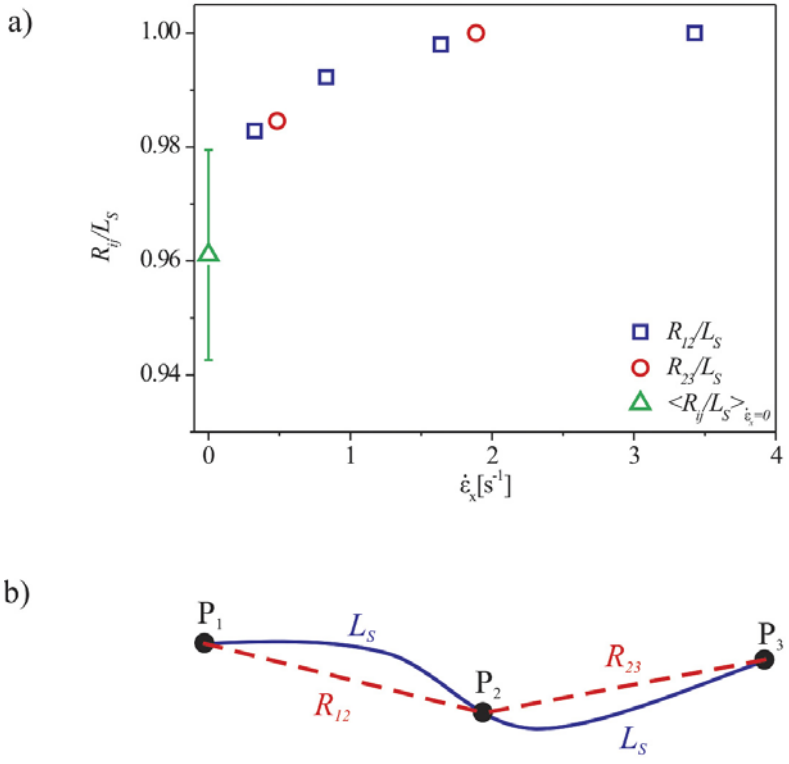

Figure 10. (a) Normalized extension R_{ij}/L_S versus strain rate calculated combining the experimental results and the simulation of figure 9. (b) Schematic diagram of the definition of R_{ij} and L_S.

leads to fluctuations around a mean extension. The 'error bar' in figure 10(a) indicates the standard deviation of the normal distribution of these fluctuations. Increasing the strain rate,

the externally applied stress suppresses the thermal fluctuations and an increased normalized extension can be found. At strain rates $\dot{\varepsilon}_x \geqslant 2\ \mathrm{s}^{-1}$ the segments are completely extended. Compared to the case for the pioneering experiments of Chu and co-workers [32, 33] on individual DNA double strands in an elongational flow with a stagnation point, our experimental set-up additionally enables a controlled interference with reactive compounds for investigations of actin filaments with actin binding and network forming proteins.

4. Conclusion and outlook

The behaviour of individual actin filaments in confining microchannels has been investigated using fluorescence microscopy and statistical analysis. Both the tangent–tangent correlation and the radial distribution function were analysed and it turns out that the microchannels act as an 'aligning guide' for the filaments. This enhances their tangent–tangent correlation and also shifts the radial distribution function towards higher values. The segments of the filaments seem to be more correlated than they actually are. We are able to describe the experimental results using a straightforward model which assumes the confining energy of the microchannels as a parabolic potential. In spite of this simplification the real conditions are fitted quite well. The filament length, L, and resulting boundary effects play an important role and have to be accounted for in a more quantitative model. We applied hydrodynamic flow stress to the filaments. This allowed us to observe the interactions of the external velocity field and the thermal fluctuations of the actin filaments. The flow suppresses the Brownian motion of the biopolymers and extends them to their full length. The use of different geometries such as curved channels or wedges and the observation of the formation of networks of actin and actin binding proteins or multivalent ions will be an important step towards a better understanding of the interplay of individual filaments and their surroundings. These investigations are not only crucial for the comprehension of the mechanical properties of the cellular processes, but also for the behaviour of dilute polymer solutions in microfluidic applications.

Acknowledgments

We gratefully acknowledge fruitful discussions with Stephan Herminghaus, Klaus Mecke, Jan Kierfeld and Holger Stark and thank Udo Krafft for excellent technical assistance. This project was supported by the DFG (Pf 375/2, Pf 375/4-1).

References

[1] Alberts B, Johnson A, Lewis J, Raff M, Roberts K and Walter P 2002 *Molecular Biology of the Cell* (New York: Garland)
[2] Le Goff L, Hallatschek O, Frey E and Amblard F 2002 *Phys. Rev. Lett.* **89** 258101
[3] Ott A, Magnasco M, Simon A and Libchaber A 1993 *Phys. Rev.* E **48** R1642
[4] Gittes F, Mickey B, Nettelton J and Howard J 1993 *J. Cell Biol.* **120** 923
[5] Isambert H, Venier P, Maggs A C, Fattoum A, Kassab R, Pantaloni D and Carlier M-F 1995 *J. Biol. Chem.* **270** 11437
[6] Käs J, Strey H, Bärmann M and Sackmann E 1993 *Europhys. Lett.* **21** 865
[7] Käs J, Strey H, Tang J X, Finger D, Ezzell R, Sackmann E and Jamney P A 1996 *Biophys. J.* **70** 609
[8] Yanagida T, Nakase M, Nishiyama K and Oosawa F 1984 *Nature* **307** 58
[9] Takebayashi T, Morita Y and Oosawa F 1977 *Biochim. Biophys. Acta* **492** 375
[10] Ishijima A, Doi T, Sakurada K and Yanagida T 1991 *Nature* **352** 301
[11] Boal D 2001 *Mechanics of the Cell* (Cambridge: Cambridge University Press)
[12] Howard J 2001 *Mechanics of Motor Proteins and the Cytoskeleton* (Sunderland: Sinauer)

[13] Pfohl T, Mugele F, Seemann R and Herminghaus S 2003 *Chem. Phys. Chem.* **4** 1291
[14] Wong I Y, Gardel M L, Reichman D R, Weeks E R, Valentine M T, Bausch A R and Weitz D A 2004 *Phys. Rev. Lett.* **92** 178101
[15] Reisner W, Morton K J, Riehn R, Wang Y M, Yu Z, Rosen M, Sturm J C, Chou S, Frey E and Austin R H 2005 *Phys. Rev. Lett.* **94** 196101
[16] Tegenfeldt J O, Prinz C, Cao H, Chou S, Reisner W W, Riehn R, Wang Y M, Cox E C, Sturm J C, Silberzan P and Austin R H 2004 *Proc. Natl Acad. Sci. USA* **101** 10979
[17] Clemmens J, Hess H, Howard J and Vogel V 2003 *Langmuir* **19** 1738
[18] Bunk R, Klinth J, Montelius L, Nicholls I A, Omling P, Tågerud S and Månsson A 2003 *Biochem. Biophys. Res. Commun.* **301** 783
[19] Landau L D and Lifshitz E M 1958 *Statistical Physics* (London: Pergamon)
[20] Kratky O and Porod G 1949 *Recl. Trav. Chim. Pay.* B **68** 1106
[21] Odijk T 1983 *Macromolecules* **16** 1340
[22] Knight J B, Vishwanath A, Brody J P and Austin R H 1998 *Phys. Rev. Lett.* **80** 3863
[23] Xia Y and Whitesides G 1998 *Annu. Rev. Matter. Sci.* **28** 153
[24] Delamarche E, Bernard A, Schmid H, Michel B and Biebuyck H 1997 *Science* **276** 779
[25] Otten A, Köster S, Struth B, Snigirev A and Pfohl T 2005 *J. Synchrotron Radiat.* **12** at press
[26] Köster S, Herminghaus S, Kierfeld J, Stark H and Pfohl T 2005 submitted
[27] Kroy K 1998 *PhD Thesis* TU München
[28] Hinner B, Tempel M, Sackmann E, Kroy K and Frey E 1998 *Phys. Rev. Lett.* **81** 2614
[29] Wilhelm J and Frey E 1996 *Phys. Rev. Lett.* **77** 2581
[30] Mecke K *et al* 2005 private communication
[31] Wagner F, Tattanzi G and Frey E 2005 private communication
[32] Perkins T T, Quake S R, Smith D E and Chu S 1994 *Science* **264** 822
[33] Perkins T T, Smith D E and Chu S 1997 *Science* **276** 2016